Improvement of Transient Response and Mitigating Current Harmonics of Grid-Tied T-Type Inverter Using Proportional Resonant Controller

Doğan Çelik
Department of Electrical and Electronics Engineering
Van Yuzuncu Yıl University
Van, Turkey
dogancelik@yyu.edu.tr

Tahsin Koroglu
Department of Electrical and Electronics Engineering
Adana Alparslan Turkes Science and Technology University
Adana, Turkey
tkoroglu@atu.edu.tr

Elanur Ekici
Department of Electrical and Electronics Engineering
Adana Alparslan Turkes Science and Technology University
Adana, Turkey
eekici@atu.edu.tr

Abstract—**This paper addresses a proportional resonant (PR) based current control scheme for a three-phase grid-connected LC-filtered three-level-T-type inverter. The proposed controller stands out for its ability to reduce total harmonic distortion (THD) of the grid current remarkably with less computational complexity. To show the effectiveness of the inverter with the developed controller, a simulation model has been created in PSCAD/EMTDC environment. The simulation results reveal that the PR controller has a fast transient response and a good reference tracking ability under dynamic conditions such as sudden changes in the reference current/power. It has been concluded that the PR controller improves the current THD better than the synchronous reference frame feed-forward decoupled PI (DQ) controller as a result of the simulation-based comparison. It has been shown that the T-type multilevel inverter is also effective in reducing the harmonic level compared to the three-phase conventional two-level inverter (TLI). The current THD is kept below 2% in compliance with the IEEE standard by using the controller and the inverter presented in this study.**

Keywords-proportional resonant controller, three-phase three-level T-Type inverter, current harmonics, grid connected inverter

I. INTRODUCTION

Power electronics converters (PECs) and control strategies are crucial for the efficient and reliable operation of renewable energy systems, electric vehicle charging systems, and industrial power supplies. Control strategies ensure that the converters operate at optimal efficiency as well as protected against various disturbances and failures. Distributed generation systems (DGSs) operate connected to (on-grid) or independent of the grid (off-grid). Among the PECs, three-phase voltage-source inverters are the most suitable solution for the connection of distributed generation systems to the three-phase grid. Voltage source inverters (VSIs) that act as interfaces between the grid and DGSs can be divided into two groups: traditional two-level inverters (TLIs) and multi-level inverters (MLIs). Compared with TLIs, MLIs have advantages such as pure output voltage waveform, high operating power range, lower switching frequency, and lower harmonic level [1]. One of the most important criteria for grid-connected converters is the total harmonic distortion (THD) value.

The MLI-based grid-tied photovoltaic (PV) system topologies with their modulation and control schemes are analyzed and investigated in [2, 3]. In [4], a three-phase neutral-point clamped (NPC) grid-connected multi-level PV inverter is investigated and a space vector modulation is applied for its controller. A three-phase three-level grid-connected NPC inverter is elaborated considering the impedance and stability characteristics in [1]. The T-type converter is one of the preferred multi-level inverter structures with its simple structure and non-isolated input DC levels [5]. Authors in [6] offer a three-level T-type quasi-Z-source grid-connected PV inverter that is managed by a modified dq control-based controller that also features an active power filter. A novel three-phase three-level T-type NPC multi-level inverter is presented for grid-tied PV-connected systems with leakage current reduction functionality in [7]. In [8], a proportional resonant (PR) based current control has been discussed for a three-phase two-leg structure T-type inverter. The THD value of the grid current is given as 2.07%. In [9], a novel switched-boost dual T-type five-level inverter for PV grid-tied applications has been introduced. The analysis and elimination of zero-sequence circulating currents in parallel three-level T-type grid-tied inverters are put forward in [10]. Several control methods such as d-q controller, PR controller, model predictive control [11], passivity-based decoupling control [12], and loss balance pulse width modulation technique [13] have been asserted for T-type grid-connected inverters. These control strategies have been proposed to manage power transfer with the grid and reduce their harmonic content on the grid side. The PR controller has been frequently used in grid-connected inverter applications due to its low current harmonic [14-18]. Another advantage regarded with the PR controller achieves implementing selective harmonic compensation with less computational complexity [19]. An overview of three-phase grid-connected inverters for renewable energy sources and a comparison and detailed analysis of the dq control and PR control methods employed in these inverters is presented in [20].

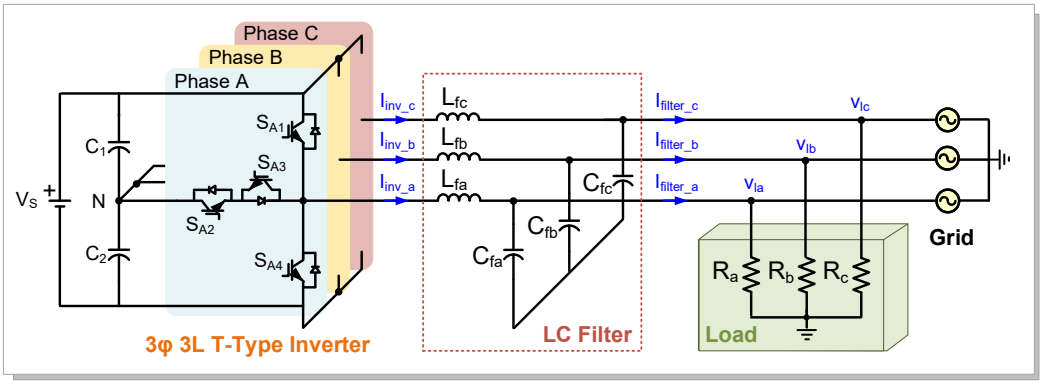

Fig.1. Topology of 3L-T-type inverter connected to the utility grid.

In this study, the operation of the three-level (3L) T-type inverter based on the comparisons of the PR controller and feed-forward decoupled PI control has been examined and tested under various cases. The PR current controller achieves lower THD, and has less control complexity. The performance of the PR control method has been addressed in case of reference power changes, dynamic response and current harmonics level. The performance of the two control methods and grid-connected T-type inverter has been verified using the PSCAD/EMTDC program. The main objectives of this paper are as follows:

i) Achieving a reduction in the THD value at the grid current by multi-level structure and PR controller according to conventional three-phase six-switch voltage-source inverter structure.

ii) Providing a comparison of the PR controller with the most widely used feed-forward decoupled PI control or dq control technique for 3L T-type inverter and conventional TLIs.

iii) Improving the performance and stability of grid-connected 3L-T-type inverter.

The paper is organized in the following manner: system design, power circuit configuration and proposed control strategies are presented in Section 2. Simulation results are provided and discussed in Section 3. The conclusions of the study are highlighted in Section 4.

II. Description And Modeling Of Grid Tied 3L-T-Type Inverter

The basic configuration of 3L-T-type inverter connected to the utility grid is depicted in Fig. 1. The dynamic model of a grid-tied 3L-T-type inverter with an LC-filter describes the behavior of the converter and its interactions with the grid and the LC filter. The 3L-T-type inverter with LC filter achieves reducing harmonic distortion and improves the power quality of the inverter's output. The model is typically represented in the dq or $\alpha\beta$ reference frame, which is a rotating reference frame that follows the power system's frequency. The model includes equations for the inverter's voltage and current control, as well as the dynamics of the LC filter [21, 22]. As given in Table I, each phase of the 3L-T-type inverter can produce three output states depending upon the upper and lower switches in each leg: "1", "0" and "-1" states. x represents a, b, c phases. Output current of 3L-T-type inverter has been generated depending on the state of the switching signals as depicted in Fig. 2.

The equations for the grid voltage and current, as well as the interactions between the inverter and the grid are expressed as follows:

$$\begin{cases} L_f \dfrac{di_{inv\_\alpha}}{dt} = v_{\alpha n} - v_{l\alpha} \\ L_f \dfrac{di_{inv\_\beta}}{dt} = v_{\beta n} - v_{l\beta} \end{cases} \quad (1)$$

$$\begin{cases} C_1 \dfrac{dv_{c1}}{dt} = i_{c1} \\ C_2 \dfrac{dv_{c2}}{dt} = i_{c2} \end{cases} \quad (2)$$

where C_1 and C_2 denote two series DC capacitors.

TABLE I. Switching States Of 3L-T-Type Inverter System

S_x	S_{x1}	S_{x2}	S_{x3}	S_{x4}	v_{xn}
1	1	1	0	0	$+v_{dc}/2$
0	0	1	1	0	0
-1	0	0	1	1	$-v_{dc}/2$

III. Control Methods

In this section, synchronous and stationary reference frame based current control methods have been analyzed. Block diagram of the control methods for the grid connected 3L-T-type inverter is shown in Fig. 3.

A. *StRF based Current Controller*

The stationary reference frame (StRF)-based control depicted in Fig. 3a is a control method that uses a fixed reference signal as the basis for control. In this approach, the control system compares the actual output of the system to the reference signal and generates a control signal to bring the output to match the reference [23]. The value of the active and reactive current components has been calculated based on given a reference for the active (p^{ref}) and reactive power (q^{ref}) in StRF as follows:

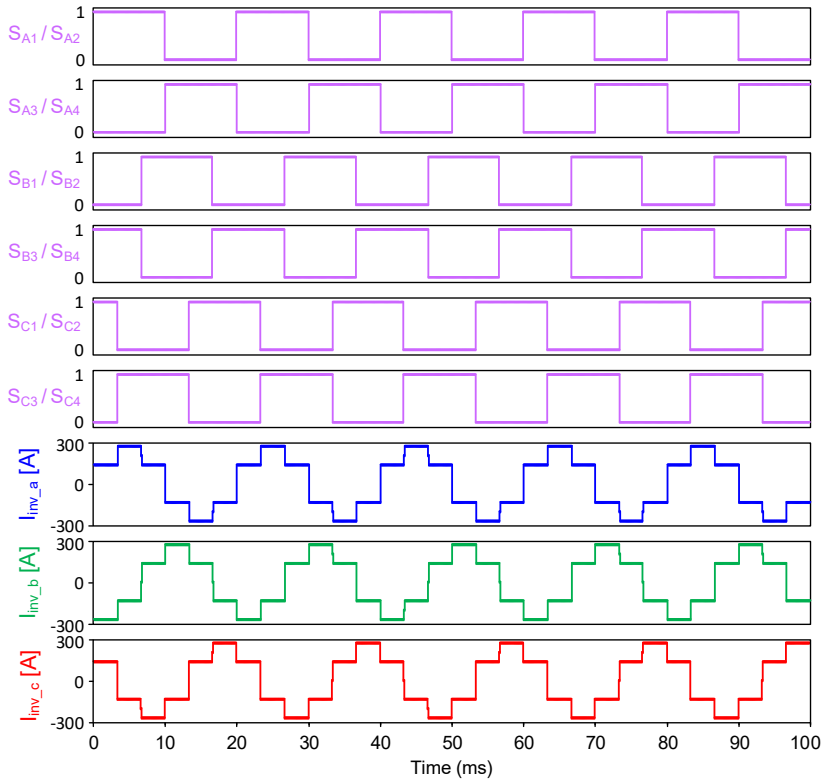

Fig.2. Gate signals and output current of 3L-T-type inverter.

$$\begin{bmatrix} i_\alpha^{ref} \\ i_\beta^{ref} \end{bmatrix}_p = \frac{1}{\Delta_{\alpha\beta}} \begin{bmatrix} v_{l\alpha} \\ v_{l\beta} \end{bmatrix} p^{ref} \tag{3}$$

where $\Delta_{\alpha\beta} = v_{l\alpha}^2 + v_{l\beta}^2$.

$$\begin{bmatrix} i_\alpha^{ref} \\ i_\beta^{ref} \end{bmatrix}_q = \frac{1}{\Delta_{\alpha\beta}} \begin{bmatrix} -v_{l\beta} \\ v_{l\alpha} \end{bmatrix} q^{ref} \tag{4}$$

The reference current is generated based on active and reactive current components as follows.

$$\begin{bmatrix} i_\alpha^{ref} \\ i_\beta^{ref} \end{bmatrix} = \begin{bmatrix} i_\alpha^{ref} \\ i_\beta^{ref} \end{bmatrix}_p + \begin{bmatrix} i_\alpha^{ref} \\ i_\beta^{ref} \end{bmatrix}_q \tag{5}$$

where i_α^{ref} and i_β^{ref} are reference current components in $\alpha\beta$ –axis.

In this subsection, a PR controller is employed in the current-control loops. The PR controller is a type of control system that consists of a combination of proportional control and resonant control to accomplish precise and stable control of a system. Proportional part uses a control signal that is proportional to the error between the desired output and the actual output of the system. On the other hand, resonant part uses a control signal that is in phase with the system's natural frequency to produce a resonant effect, which can enhance the system's stability and response time. The proportional part of the PR controller is employed to control the output voltage by adjusting the duty cycle of the inverter switch [22-28]. The PR control can be useful in many applications such as renewable energy systems, electric vehicle charging systems, and industrial power supplies. The combination of proportional and resonant control parts can achieve high-precision control over the output voltage and frequency, leading to efficient and stable operation of the system. The transfer function of the PR control is expressed by (6).

$$\begin{aligned} G_{PR}(s) = G_P(s) + G_R(s) &= \kappa_p + \kappa_r \frac{2(\Omega_c s + \Omega_c^2)}{s^2 + 2\Omega_c s + (\Omega_c^2 + \Omega^2)} \\ &\approx \kappa_p + \kappa_r \frac{2\Omega_c s}{s^2 + 2\Omega_c s + \Omega^2} \end{aligned} \tag{6}$$

where κ_p and κ_r are proportional and resonant parts of the PR controller. Ω_c and Ω represents cut-off frequency and grid frequency, respectively. The design of the PR controller can be given as: i) a suitable value of Ω_c is selected to provide a bandwidth close to the resonant frequency. ii) κ_p is selected to provide good transient response and to enhance stability of the system. iii) κ_r is selected to eliminate magnitude and phase steady-state errors. $\Omega_c = 2\pi f_0 \Delta f_0$, Δf_0 is the limit of variation of the fundamental frequency. $\kappa_p = 8L_f/3T_s$ [29].

B. SyRF based Current Controller

Synchronous reference frame (SyRF) based feed-forward decoupled PI control shown in Fig. 3b is a control technique that employed in electrical systems, such as motor and wind energy conversion systems, to improve performance and stability [30]. It utilizes a SyRF to convert the dynamics of the system into a rotating reference frame, which permits for decoupling the control of the active and reactive power components. SyRF based feed forward decoupled PI control equations are written by (7) and (8) [31, 32].

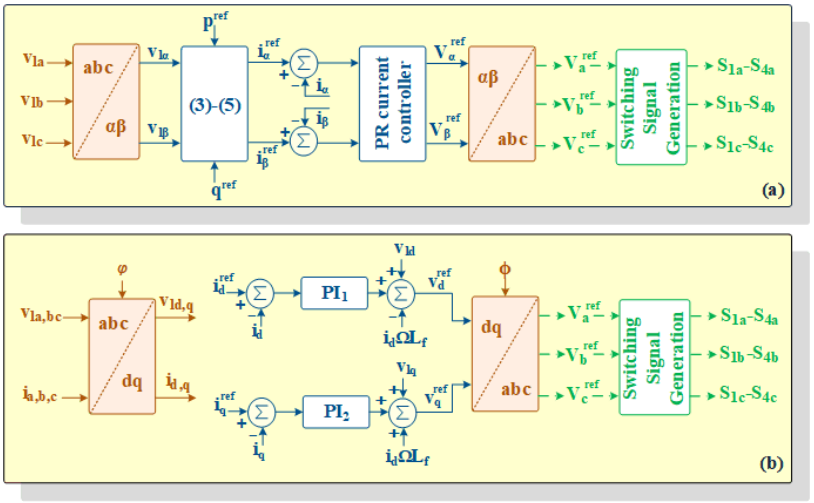

Fig. 3. Control block diagram of the grid connected 3L-T-type inverter; a) StRF based current controller and SyRF based current controller.

$$\begin{cases} \dfrac{dv_d^*}{dt} = \kappa_{i,1}(i_d^{ref} - i_d) \\ \dfrac{dv_q^*}{dt} = \kappa_{i,2}(i_q^{ref} - i_q) \end{cases} \tag{7}$$

where i_d^{ref} and i_q^{ref} are reference active and reactive current components in dq-axis. $\kappa_{i,1}$ and $\kappa_{i,2}$ represents the integral gain of the PI controllers. The reference voltage has been derived by [22] to generate switching signals of 3L-T-type inverter.

$$\begin{cases} v_d^{ref} = \kappa_{p,1}(i_d^{ref} - i_d) - j\Omega L_f i_q + v_d^* \\ v_d^{ref} = \kappa_{p,2}(i_q^{ref} - i_q) + j\Omega L_f i_d + v_q^* \end{cases} \tag{8}$$

where $\kappa_{p,1}$ and $\kappa_{p,2}$ denotes the proportional gains of the PI controllers.

IV. Results And Discussion

The performance of the three-phase 3L-T-type inverter and its controller has been tested by simulation results performed in PSCAD/EMTDC. The design parameters of the simulation model are summarized in Table II. The effectiveness of the system has been validated through different case studies involving current injection into the grid, current drawing from the grid, and step changes in reference current.

Fig. 4 presents the simulation waveform corresponding to the current injection into the grid for phase-A. In this case, the grid current (I_{filter_a}) is in phase with the grid voltage (V_{grid_a}). As seen from the Fig.4, the reference current is 50 A and the THD of the grid current is recorded as 1.81 %.

The dynamic response of the inverter is tested under step changes in the reference grid current. The first case explores the behavior of the controller under a sudden decrease in the reference current. Fig. 5 shows that the peak value of the inverter output current injected into the grid reduces from 300 A to 150 A at t=0.5 s. It has been seen that the PR controller provides a fast transient response and the inverter is able to reach a steady state quickly. The filtered inverter currents (I_{filter_a}, I_{filter_b}, I_{filter_c}) are in phase with the grid voltages (V_{grid_a}, V_{grid_b}, V_{grid_c}) and a unity power factor is achieved.

TABLE II. The Parameters of The Simulation Model

Parameters	Values
DC link (input) voltage (V_s)	800 V
DC link capacitors (C_1 and C_2)	470 µF
Output filter inductors (L_{fa}, L_{fb}, L_{fc})	1.5 mH
Output filter capacitors (C_{fa}, C_{fb}, C_{fc})	10 µF
Switching Frequency (f_{sw})	2500 Hz
Rated Power (P_{inv})	300 kW
Proportional and resonant gains (K_p, K_r))	100, 0.00001
Load ($R_{a,b,c}$)	10Ω

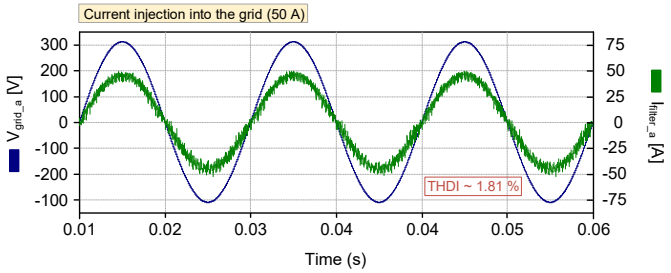

Fig. 4. Current injection into the grid (50 A current reference).

The THD of the grid current rises from 0.86 % to 1.72 % during the current reference change. In the second case study, the transition from the current injecting mode to the current drawing mode and the sudden increase in the reference current are investigated. The simulation waveforms of the grid current and grid voltage are depicted in Fig. 6. It is obvious that the inverter injects 100 A into the grid until t=0.5 and after that time 200 A is drawn from the grid. The phase difference between the grid current and the grid voltage is 180° when the current is drawn from the grid. Similar to the first case study, the controller's response to the sudden change in reference current is fast enough.

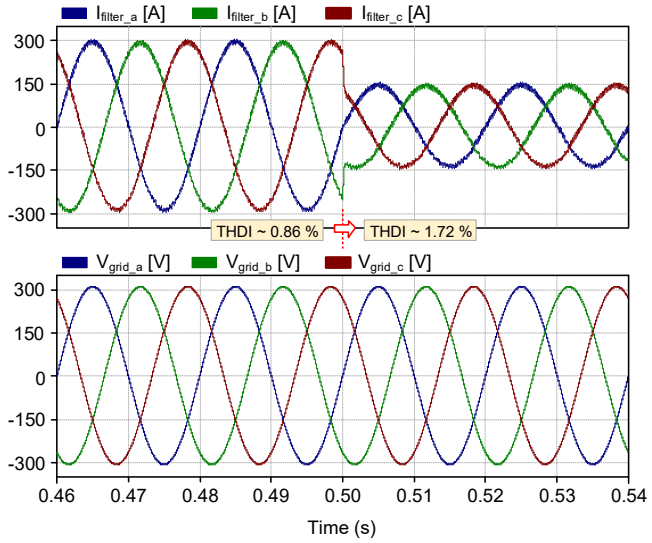

Fig. 5. Step decrease in injected current reference (from 300 A to 150 A).

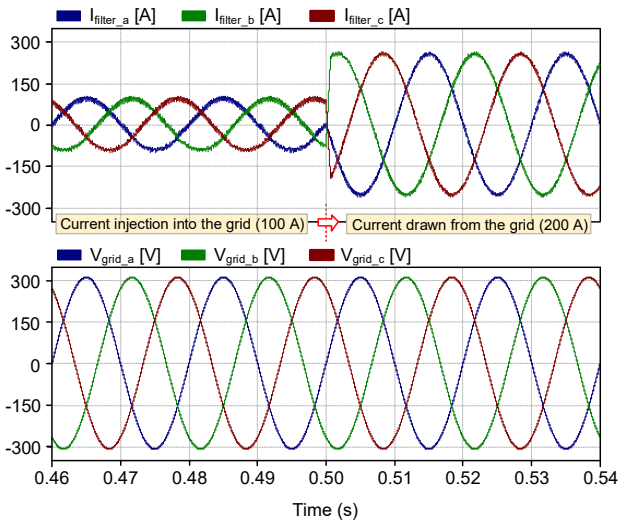

Fig. 6. Step increase in the current reference and transition from the injecting mode to the drawing mode.

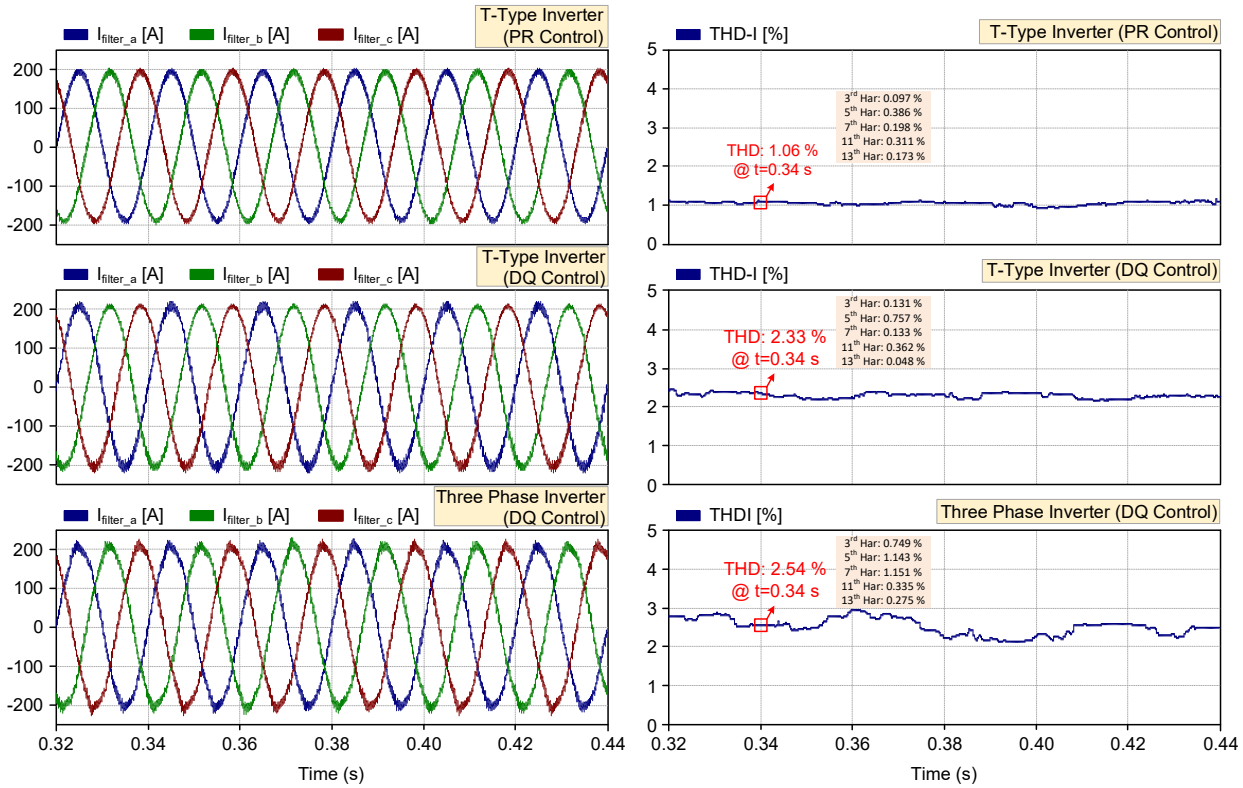

Fig. 7. A performance comparison between StRF based PR and SyRF based feed-forward decoupled PI (DQ) controllers.

In Fig. 7, StRF based PR controller developed for a three-phase 3L-T-type inverter is compared with the traditional SyRF based feed-forward decoupled PI (DQ) controller, which is applied in the same type of inverter and in the conventional three-phase TLIs. The waveform of the grid currents and the obtained current THD values are demonstrated in Fig. 7. As can be understood from the figure, the three-phase three-level 3L-T-type inverter with the PR controller has the lowest current THD.

V. CONCLUSIONS

In this paper, a performance comparison between StRF based PR and SyRF based feed-forward decoupled PI controllers has been fulfilled for 3L-T-type inverter. In terms of performance evaluation of the 3L-T-type inverter and two-

conventional TLIs, the T-type inverter typically have lower THD and less harmonic distortion, while the conventional inverter have higher THD and more harmonic distortion. Comparative verification results show that the THD by StRF based PR controller has remained around ∼1.0%, while the conventional approach could contain the distortion to around ∼2.25% in some cases only. The StRF based PR controller of the 3L-T-type inverter provides a fast transient response and is able to reach a steady state quickly. The effectiveness and performances of the proposed control methods have been confirmed by computer simulations under several cases.

REFERENCES

[1] B. Zhang, X. Du, J. Zhao, J. Zhou, X. Zou, "Impedance modeling and stability analysis of a three-phase three-level NPC inverter connected to the grid," CSEE J. Power Energy Syst., vol. 6, no. 2, pp. 270-278, 2020.

[2] A. Sinha, K.C. Jana, M. K. Das, "An inclusive review on different multi-level inverter topologies, their modulation and control strategies for a grid connected photo-voltaic system," Sol. Energy, vol. 170, pp. 633-657, 2018.

[3] S. Mehta, V. Puri, "A Review of different multi-level inverter topologies for grid integration of solar photovoltaic system," Renew. Energy Focus, vol. 43, pp. 263-276, December 2022.

[4] K. Arulkumar, D. Vijayakumar, K. Palanisamy, "Modeling and control strategy of three phase neutral point clamped multilevel PV inverter connected to the grid," J. Build. Eng., vol. 3, pp. 195-202, 2015.

[5] K. K. Gupta, A. Ranjan, P. Bhatnagar, L. K. Sahu, S. Jain, "Multilevel inverter topologies with reduced device count: A review," IEEE Trans. Power Electr., vol. 31, no. 1, pp. 135-151, 2015.

[6] F. Barrero-González, C. Roncero-Clemente, J. Gutiérrez-Escalona, M. I. Milanés-Montero, E. González-Romera, E. Romero-Cadaval, "Three-level T-type quasi-Z source pv grid-tied inverter with active power filter functionality under distorted grid voltage," IEEE Access, vol. 10, pp. 44503-44516, 2022.

[7] P. Madasamy, V. Suresh Kumar, P. Sanjeevikumar, J. B. Holm-Nielsen, E. Hosain, C. Bharatiraja, "A three-phase transformerless T-Type-NPC-MLI for grid connected PV systems with common-mode leakage current mitigation. Energies, vol. 12, no. 12, pp. 2434, 2019.

[8] N. Altin, I. Sefa, H. Komurcugil, S. Ozdemir, "Three-phase three-level T-type grid-connected inverter with reduced number of switches," In 2018 6th International Istanbul Smart Grids and Cities Congress and Fair (ICSG), pp. 58-62, April 2018.

[9] R. Barzegarkhoo, S. S. Lee, Y. P. Siwakoti, S. A. Khan, F. Blaabjerg, "Design, control, and analysis of a novel grid-interfaced switched-boost dual T-type five-level inverter with common-ground concept," IEEE Trans. Ind. Electron., vol. 68, no. 9, pp. 8193-8206, 2020.

[10] Z. Shao, X. Zhang, F. Wang, R. Cao, "Modeling and elimination of zero-sequence circulating currents in parallel three-level T-type grid-connected inverters," IEEE Trans. Power Electron., vol. 30, no. 2, pp. 1050-1063, 2014.

[11] G. Yang, S. Hao, C. Fu, Z. Chen, "Model predictive direct power control based on improved T-type grid-connected inverter," IEEE Trans. Emerg. Sel., vol. 7, no. 1, pp. 252-260, 2018.

[12] J. Wang, X. Mu, Q. K. Li, "Study of passivity-based decoupling control of T-NPC PV grid-connected inverter. IEEE Trans. Ind. Electron., vol. 64, no. 9, pp. 7542-7551, 2017.

[13] M. Aly, E. M. Ahmed, M. Shoyama, "Modulation method for improving reliability of multilevel T-type inverter in PV systems. IEEE Trans. Emerg. Sel., vol. 8, no. 2, pp. 1298-1309, 2019.

[14] H. D. Tafti, A. I. Maswood, A. Ukil, O. H. Gabriel, L. Ziyou, "NPC photovoltaic grid-connected inverter using proportional-resonant controller," In 2014 IEEE PES Asia-Pacific Power and Energy Engineering Conference (APPEEC), pp. 1-6, December 2014.

[15] O. Husev, C. Roncero-Clemente, E. Makovenko, S. P. Pimentel, D. Vinnikov, J. Martins, "Optimization and implementation of the proportional-resonant controller for grid-connected inverter with significant computation delay," IEEE Trans. Ind. Electron., vol. 67, no. 2, pp. 1201-1211, 2019.

[16] X. Quan, "Improved dynamic response design for proportional resonant control applied to three-phase grid-forming inverter. IEEE Trans. Ind. Electron., vol. 68, no. 10, pp. 9919-9930, 2020.

[17] H. Komurcugil, N. Altin, S. Ozdemir, I. Sefa, "Lyapunov-function and proportional-resonant-based control strategy for single-phase grid-connected VSI with LCL filter. IEEE Trans. Ind. Electron., vol. 63, no. 5, pp. 2838-2849, 2015.

[18] P. K. Kar, A. Priyadarshi, S. B. Karanki, "Control strategy for single-phase grid-interfaced modified multilevel inverter topology for distributed power generation," IEEE Syst. J., vol. 16, no. 1, pp. 1627-1636, 2021.

[19] R. Teodorescu, F. Blaabjerg, M. Liserre, P. C. Loh, "Proportional-resonant controllers and filters for grid-connected voltage-source converters. IEE Proc., Electr. Power Appl., vol. 153, no. 5, pp. 750-762, 2006.

[20] N. F. Guerrero-Rodríguez, A. B. Rey-Boué, E. Reyes-Archundia, "Overview and comparative study of two control strategies used in 3-phase grid-connected inverters for renewable systems," Renew. Energy Focus, vol. 19, pp. 75-89, 2017.

[21] N. Baeckeland, D. Venkatramanan, M. Kleemann, S. Dhople, "Stationary-frame grid-forming inverter control architectures for unbalanced fault-current limiting," IEEE Trans. Energy Convers., vol. 37, no. 4, 2813-2825, 2022.

[22] Y. Yu, X. Hu, "Active disturbance rejection control strategy for grid-connected photovoltaic inverter based on virtual synchronous generator," IEEE Access, vol. 7, pp. 17328-17336, 2019.

[23] X. Yan, M. Cheng, "Backstepping-based direct power control for dual-cage rotor brushless doubly fed induction generator," IEEE Trans. Power Electron., vol. 38, no. 2, pp. 2668-2680, 2022.

[24] P. Montero-Robina, K. Rouzbehi, F. Gordillo, J. Pou, "Grid-following voltage source converters: Basic schemes and current control techniques to operate with unbalanced voltage conditions," IEEE open J. Ind. Electron. Soc., vol. 2, pp. 528-544, 2021.

[25] N. Baeckeland, D. Venkatramanan, M. Kleemann, S. Dhople, "Stationary-frame grid-forming inverter control architectures for unbalanced fault-current limiting," IEEE Trans. Energy Convers., vol. 37, no. 4, pp. 2813-2825, 2022.

[26] H. Ahmed, D. Çelik, "Sliding mode based adaptive linear neuron proportional resonant control of Vienna rectifier for performance improvement of electric vehicle charging system," J. Power Sources, vol. 542, pp. 231788, 2022.

[27] M. E. Meral, D. Çelik, "Comparison of SRF/PI-and STRF/PR-based power controllers for grid-tied distributed generation systems. Electr. Eng., vol. 100, no. 2, pp. 633-643, 2018.

[28] B. Fan, X. Wang, "A Lyapunov-based nonlinear power control algorithm for grid-connected VSCs," IEEE Trans. Ind. Electron., vol. 69, no. 3, pp. 2916-2926, 2021.

[29] T. Ye, N. Dai, C. S. Lam, M. C. Wong, J. M Guerrero,. "Analysis, design, and implementation of a quasi-proportional-resonant controller for a multifunctional capacitive-coupling grid-connected inverter," IEEE Transactions on Industry Applications, vol. 52, no. 5, pp. 4269-4280, 2016.

[30] L. Guo, R. Liu, X. Li, Y. Zhang, "Neutral point potential balancing method for three-level power converters in two-stage three-phase four-wire power conversion system," IET Power Electron., vol. 13, no. 12, pp. 2618-2627, 2020.

[31] E. Avci, M. Ucar, "Proportional multi-resonant-based controller design method enhanced with a lead compensator for stand-alone mode three-level three-phase four-leg advanced T-NPC inverter system," IET Power Electron., vol. 13, no. 4, pp. 863-872, 2020.

[32] J. Gutiérrez-Escalona, C. Roncero-Clemente, O. Husev, F. Barrero-González, A. M. Llor, V. F. Pires, "Three-Level T-Type qZ Source Inverter as Grid-Following Unit for Distributed Energy Resources," IEEE Trans. Emerg. Sel., vol. 10, no. 6, pp. 7772-7785, 2022.